AGU PUBLICATIONS

Water Resources Research

RESEARCH ARTICLE
10.1002/2014WR016139

Special Section:
Connectivity, Non-Linearity, and Regime Transitions in Future Earthscapes

Dynamic connectivity in a fluvial network for identifying hotspots of geomorphic change

Jonathan A. Czuba[1] and Efi Foufoula-Georgiou[1]

[1]Department of Civil, Environmental, and Geo- Engineering, St. Anthony Falls Laboratory, National Center for Earth-Surface Dynamics, University of Minnesota, Minneapolis, Minnesota, USA

Key Points:
- Assess flux organization on a river network via a dynamic connectivity framework
- Track how mass clusters and persists during transport on a network
- Persistent sediment clusters coincide with observed channel-migration hotspots

Supporting Information:
- Supporting Information S1
- Movie S1

Correspondence to:
E. Foufoula-Georgiou,
efi@umn.edu

Citation:
Czuba, J. A., and E. Foufoula-Georgiou (2015), Dynamic connectivity in a fluvial network for identifying hotspots of geomorphic change, *Water Resour. Res.*, *51*, 1401–1421, doi:10.1002/2014WR016139.

Received 15 JUL 2014
Accepted 17 JAN 2015
Accepted article online 28 JAN 2015
Published online 2 MAR 2015

Abstract Dynamical processes occurring on the hierarchical branching structure of a river network tend to heterogeneously distribute fluxes on the network, often concentrating them into "clusters," i.e., places of excess flux accumulation. Here, we put forward the hypothesis that places in the network predisposed (due to process dynamics and network topology) to accumulate excess sediment over a considerable river reach and over a considerable period of time reflect locations where a local imbalance in sediment flux may occur thereby highlighting a susceptibility to potential fluvial geomorphic change. We develop a dynamic connectivity framework which uses the river network structure and a simplified Lagrangian transport model to trace fluxes through the network and integrate emergent "clusters" through a cluster persistence index (CPI). The framework was applied to sand transport in the Greater Blue Earth River Network in the Minnesota River Basin. Three hotspots of fluvial geomorphic change were defined as locations where high rates of channel migration were observed and places of high CPI coincided with two of these hotspots of possibly sediment-driven change. The third hotspot was not identified by high CPI, but instead is believed to be a hotspot of streamflow-driven change based on additional information and the fact that high bed shear stress coincided with this hotspot. The proposed network-based dynamic connectivity framework has the potential to place dynamical processes occurring at small scales into a network context to understand how reach-scale changes cascade into network-scale effects, useful for informing the large-scale consequences of local management actions.

1. Introduction

River basins are drained by networks of hierarchically connected channels which serve as the primary pathways for transport of environmental fluxes. The branching network structure (defined here by the network topology and its associated geometry, i.e., link lengths) serves as a template upon which environmental fluxes of water, sediment, nutrients, etc. are conveyed and organized both spatially and temporally within the basin. It has been recognized that the river network plays a central role in structuring ecosystem processes and functions by heterogeneously distributing fluxes on the network often leading to critical places and times where excess fluxes accumulate or altered system functionality emerges [e.g., *Benda et al.*, 2004a; *Campbell Grant et al.*, 2007; *Carrara et al.*, 2012; *McCluney et al.*, 2014]. This emergent behavior is difficult to predict with reductionist approaches, e.g., too detailed, fine resolution, small spatial and temporal extent, and overparameterized physically based models, and requires simpler system-level models that capture the essential elements of the system.

Such system-based conceptual models, which explicitly consider the network structure and simplified process dynamics have been at the heart of hydrologic response frameworks. Major advances include the development of the instantaneous unit hydrograph (IUH) and geomorphologic IUH theories [e.g., *Rodriguez-Iturbe and Valdes*, 1979; *Gupta et al.*, 1980], the width function formulation of the unit hydrograph [e.g., *Kirkby*, 1976; *Troutman and Karlinger*, 1985; *Gupta et al.*, 1986; *Mesa and Mifflin*, 1986; *Marani et al.*, 1991], river network transport models based on stochastic Kolmogorov equations [e.g., *Gupta et al.*, 1986; *Rinaldo et al.*, 1991; *Marani et al.*, 1991], and also theories of scaling of the hydrologic response [e.g., *Mantilla et al.*, 2006; *Furey and Gupta*, 2007; *Gupta et al.*, 2010]. Apart from the flux of water, similar concepts of system response have also been used for the computation of fluxes of sediment [e.g., *Lee and Yang*, 2010; *Czuba and Foufoula-Georgiou*, 2014] as well as nutrients [e.g., *Botter et al.*, 2006; *Rinaldo et al.*, 2006] at the outlet of a basin. These system-based conceptual models allow investigation of emergent behavior in terms of the timing and magnitude of peak response of a flux as well as tracing the origin of that flux from disparate

basin-wide contributions [e.g., see *Czuba and Foufoula-Georgiou*, 2014 for a recent application]. However, focusing on the response at the basin outlet only does not help in identifying where and when critical hotspots, defined as places of excess flux accumulation, might emerge on the network.

Identification of hotspots on a river network requires a model that tracks a flux explicitly on the river network, providing a continuous description of its spatiotemporal evolution at all locations and all times. Such an approach often necessitates simplifying the process dynamics in order to model the flux at the basin scale and over long periods of time. A number of models exist that explicitly track a flux on the river network focusing on bed-material sediment [*Benda and Dunne*, 1997; *Benda et al*., 2004b], nitrate and denitrification [*Alexander et al*., 2009], phytoplankton and nutrient limitation on biomass [*Istvánovics et al*., 2014], invasion of zebra mussels [*Mari et al*., 2011], spreading of cholera [*Bertuzzo et al*., 2008], distribution of benthic invertebrates [*Ceola et al*., 2014], and distribution of biodiversity of freshwater fish species [*Muneepeerakul et al*., 2008; *Bertuzzo et al*., 2009]. While not an explicit focus of these models, it is argued here that the space-time distribution of a flux on the network generated by these models can be used to identify hotpots.

In this paper, we are mostly concerned about identifying hotspots of fluvial geomorphic change. Fluvial geomorphic change (e.g., changes to channel planform, channel width, roughness, or slope) often occurs where there is a local imbalance of sediment and water fluxes, conceptually embodied through (an expanded) Lane's balance [e.g., *Dust and Wohl*, 2012]. This imbalance drives fluvial geomorphic change through physical mechanisms such as bank erosion, channel incision, and aggradation. Hotspots of fluvial geomorphic change are then locations where these changes are occurring at much higher rates than are occurring throughout the rest of the basin. The identification of potential hotspots of fluvial geomorphic change at the network scale has only focused on identifying confluences susceptible to change based on their position in the network [e.g., *Benda et al*., 2004a, 2004b]. These works are an important step forward, but much can still be learned by incorporating simplified process-dynamics that would allow assessment of changes that may occur in specific river reaches rather than just at confluences.

A specific type of fluvial geomorphic change associated with a change in channel planform is channel migration. Channel migration has been described as being driven by one of two mechanisms depending on whether outer bank erosion or inner bank deposition is taking the lead: (1) streamflow-driven bank-pull, i.e., more rapid erosion of the outer bank forcing deposition on the point bar along the inner bank, and (2) sediment-driven bar-push, i.e., more rapid accretion of the point bar along the inner bank forcing erosion of the outer bank [*Parker et al*., 2011; *van de Lageweg et al*., 2014; *Eke et al*., 2014]. The identification of hotspots of channel migration has typically been limited to pinpointing specific bends of river reaches [e.g., *Lagasse et al*., 2004; *Abad and Garcia*, 2006; *Motta et al*., 2012]. However, in the larger spatial context of a river network, we hypothesize that it may be possible to identify hotspots of channel migration driven by the bar-push mechanism by identifying reaches where sediment persists within a river network. This hypothesis forms the basis of this work and it is tested using a simplified model of transport and independently collected field observations of channel migration.

In our previous work [*Czuba and Foufoula-Georgiou*, 2014], we developed a network-based, sediment-transport model following a Lagrangian perspective and used it to compute the sedimentograph at the outlet of a basin (defined as the sediment response function to a uniformly distributed input of sediment throughout the basin). In this paper, we extend this framework to interrogate the system not only at its outlet response but also within it, i.e., its internal dynamics. That is, we seek to understand how sediment is organized and where sediment accumulates due to the combined effects of transport dynamics (accounting for slopes, channel morphology, bed shear stress, grain size, etc.) and river network structure (topology and associated geometry). Specifically, we present a dynamic connectivity framework for describing the organization of a flux on a network (section 2) and then apply this framework to sand transport in the Greater Blue Earth River Basin in Minnesota (section 3). We show how this framework can be used to assess the persistence of mass within different reaches of a network and ultimately identify hotspots of fluvial geomorphic change associated with observed high rates of channel migration (section 4). This framework was then used to pinpoint the sources of sediment contributing to large clusters which can be useful information for management decisions (section 5). Finally, we close with some concluding remarks (section 6).

2. Dynamic Connectivity Framework

The term "connectivity" as applied in geomorphology and hydrology has had a number of different definitions (for a review of recent literature addressing hydrological connectivity see *Bracken et al*. [2013] and sediment connectivity see *Bracken et al*. [2015] and also *Heckmann et al*. [2015]). In the context of sediment connectivity, these definitions generally refer to the degree to which sediment is able to move between different landscape features. Most recently, *Bracken et al*., [2015] defines "sediment connectivity" as, "the integrated transfer of sediment across all possible sources to all potential sinks in a system over the continuum of detachment, transport, and deposition, which is controlled by how the sediment moves between all geomorphic zones: on hillslopes, between hillslopes and channels, and within channels." Herein we use the term "connectivity" in the general sense of the definition as "being connected" and apply it in the context of fluxes on a network. We consider two fluxes "connected" if they are in close spatial proximity along the river network (how close is close enough is discussed in sections 2.3 and 3.3) and refer to "connectivity" as the state of two or more fluxes being connected. Then by "dynamic connectivity" we refer to how the connectivity of fluxes changes in time.

The proposed framework for considering the dynamic connectivity of a flux involves establishing the network (section 2.1), tracking a flux on the network (section 2.2), and then quantifying the dynamic connectivity of the flux from its spatial organization on the network (section 2.3). The flux we consider herein is sand, i.e., sediment with grain size of 0.062–2 mm.

2.1. River Network

Let the river network be defined as a directed network of connected links where direction of flow is uniquely defined. Each link i represents a segment of the river network between a source and a junction (a source link), two successive junctions, or a junction and the basin outlet. Junctions are the points at which two links join and connect to one downstream link, sources are the points farthest upstream in the network, and the outlet is the point farthest downstream in the network. Each link i is assigned a "geomorphic state" ξ_i with physical attributes corresponding to that state. Although this framework can be used for any connected flow paths (e.g., hillslope or subsurface paths), herein we only consider a fluvial channel network, thus every link corresponds to the geomorphic fluvial state $\xi_{f,i}$ with geomorphologic and hydraulic attributes of the link (Figure 1a), i.e., $\xi_{f,i}\left(\ell_i, a_i, A_i, S_i, Q_{w,i}, H_i, B_i, \ldots\right)$, where the geomorphologic attributes include link length ℓ_i (L), directly contributing area a_i (L^2), upstream drainage area A_i (L^2), and link slope S_i; and the hydraulic attributes include streamflow $Q_{w,i}$ (L^3T^{-1}), cross-section average depth H_i (L), width B_i (L), etc. While not indicated explicitly, attributes of the geomorphic fluvial state $\xi_{f,i}$ may also be a function of time to capture possible time-varying properties of the system.

2.2. Transport Dynamics

The theoretical basis of the proposed transport formulation rests on the link between Eulerian and Lagrangian transport formalisms by which one can establish the relation between the space-time trajectories of an ensemble of inputs to the network at an initial time to the arrival (or travel) time distribution at a fixed location [e.g., *Rinaldo and Rodriguez-Iturbe*, 1996]. The proposed framework uses a Lagrangian formulation of transport where "parcels" are injected at different locations in the basin at an initial time t_0 and their trajectories are followed over space and time. A parcel is a fundamental unit transported on the network and represents a collection of particles that can be physically treated as a coherent unit. Adopting established notation, let us denote by $m(\boldsymbol{X}_0, t_0)$ the initial mass of a parcel injected at time t_0 at an initial position $\boldsymbol{X}_0 = \boldsymbol{X}(t_0)$ and let $\boldsymbol{X}(t)$ denote its trajectory defined by the Lagrangian coordinate of the parcel at time t. Acknowledging uncertainties and natural variability in the transport process, the trajectory $\boldsymbol{X}(t)$ of a parcel can be seen as a random function $g(\boldsymbol{X}, t)$, called the displacement probability density function (pdf), where $g(\boldsymbol{X}, t)d\boldsymbol{X}$ characterizes the probability that a parcel is in location $(\boldsymbol{X}-d\boldsymbol{X}, \boldsymbol{X}+d\boldsymbol{X})$ at time t [e.g., *Rinaldo and Rodriguez-Iturbe*, 1996]. Considering an ensemble of parcels traveling over different pathways along the branching river network, the travel time formulation of the hydrologic response relies on establishing the relation between the displacement pdf $g(\boldsymbol{X}, t)$ and the travel time pdf $f(t)$ at a fixed control section, here the outlet of a basin, although any point in the basin can act as the outlet of a smaller subbasin. To establish this relation, first we must define a fixed control section in the transport volume V (L^3) such that all parcels injected into V are transported past the control section. The arrival time T (T) of a parcel at the control section is also a random variable characterized by the

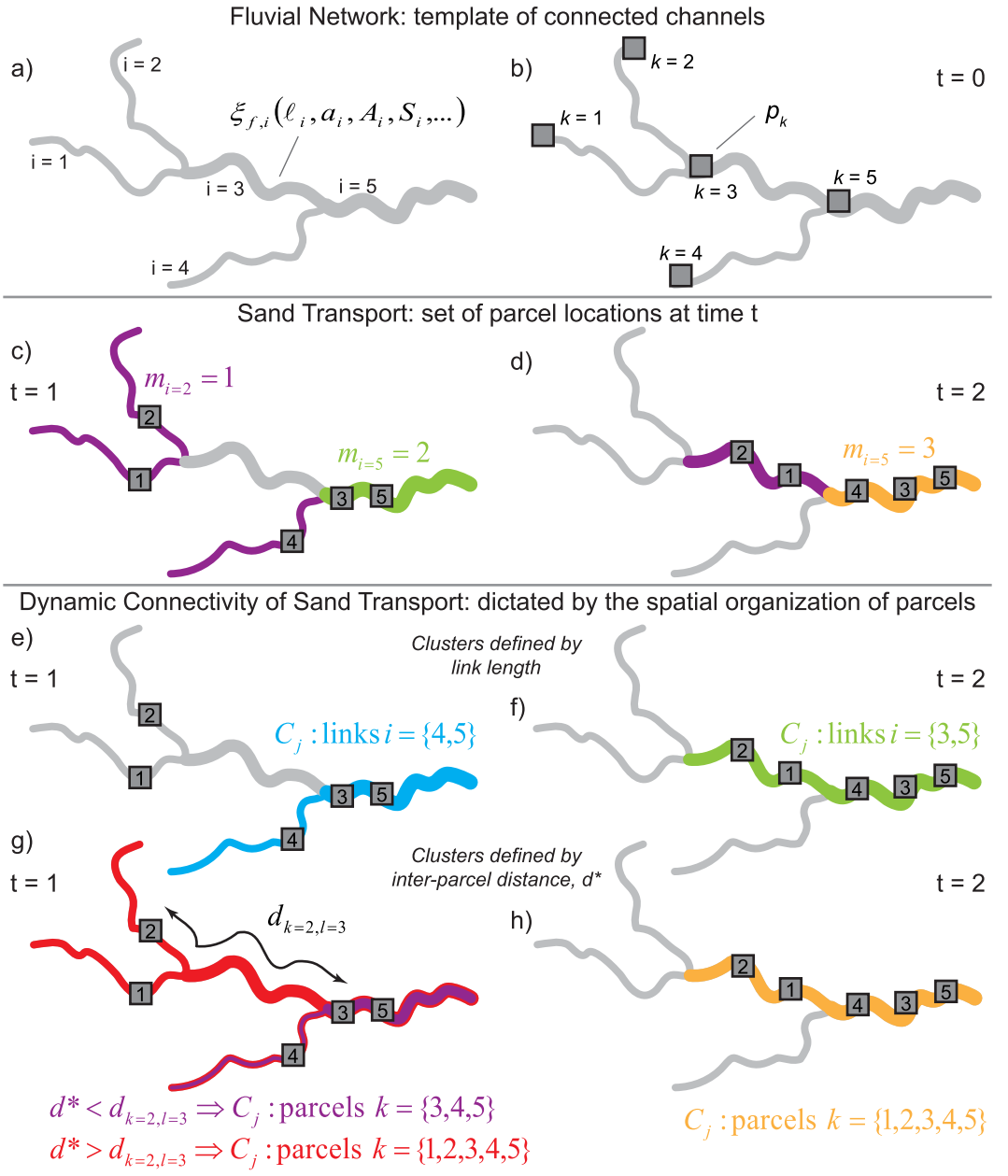

Figure 1. Overview of the dynamic connectivity framework. The framework involves: (a) establishing the river network where each link i is assigned a fluvial geomorphic state $\xi_{f,i}$; (b) tracking a flux on the network as a set of locations of the parcels p_k (each of mass $m = 1$) on the network, shown here at times $t = 0$, (c) $t = 1$, and (d) $t = 2$; and then quantifying the dynamic connectivity of the flux from the spatial organization of the parcels on the network, shown as clusters C_j defined by both link length at times (e) $t = 1$ and (f) $t = 2$ and also interparcel distance (d^*) at times (g) $t = 1$ and (h) $t = 2$. See text for cluster definitions.

probability that a parcel originating from $\boldsymbol{X}_0$ at t_0 has already crossed the control section at time t, i.e., $P(T < t) = P(t; \boldsymbol{X}_0, t_0)$. Eulerian and Lagrangian approaches are thus linked as

$$P(T < t) = 1 - \int_V g(\boldsymbol{X}, t; \boldsymbol{X}_0, t_0)\ d\boldsymbol{X}, \tag{1}$$

where the travel time pdf is given by

$$f(t) = \frac{dP(T < t)}{dt}. \tag{2}$$

A detailed account of this development has been described by *Rinaldo and Rodriguez-Iturbe* [1996].

We consider an instantaneous and spatially uniform input of sediment throughout the basin; this allows us to probe the system and quantify its response and the space-time organization of fluxes that emerges as a system property due to network topology and process dynamics. In other words, a uniform input transported though the network will reveal the system predisposition for recurring local patterns and locations where flux accumulates and persists, important indicators of sediment-driven fluvial geomorphic change. For simplicity, we attribute the instantaneous spatially uniform input of sediment to the basin as an instantaneous input at the upstream end of every link. Although the directly contributing area to every link might differ and thus the quantity of sediment input to every link might be spatially variable, here we assume it constant (without loss of generality) and call each input a "parcel" of sediment (with each parcel indexed by a unique index k) as p_k all with the same mass m (M) (Figure 1b). In other words, each parcel represents a hillslope contribution of sediment associated with the link in which the parcel was first introduced.

The Lagrangian framework of transport moves all these instantaneously released parcels at time $t=t_0$ through the network according to the specific process dynamics. At every time t, we track the location of each parcel p_k, i.e., its Lagrangian trajectory $\boldsymbol{X}_{p_k}(t)$. If the original river network has N links, then N parcels $p_1, p_2, \ldots, p_N$ were released at time $t=t_0$ at locations $\boldsymbol{\chi}_0(t_0)=\{\boldsymbol{X}_{p_1}(t_0), \boldsymbol{X}_{p_2}(t_0), \ldots, \boldsymbol{X}_{p_N}(t_0)\}$, which in our case are the coordinates of the upstream junctions of all links. As the parcels move downstream, at any time t we will have a collection of Lagrangian parcel locations as $\boldsymbol{\chi}(t)=\{\boldsymbol{X}_{p_1}(t), \boldsymbol{X}_{p_2}(t), \ldots, \boldsymbol{X}_{p_N}(t)\}$. Through transport on the hierarchical branching river network, these parcels become spatially organized and this organization changes dynamically over time (Figures 1c and 1d). This set of parcel trajectories embeds a measure (here parcel mass m at locations $\boldsymbol{\chi}(t)$ and 0 everywhere else) on the underlying network. For each link, we can then compute the total mass $m_i(t)$ in link i at time t as

$$m_i(t)=\sum_{\substack{\text{parcels } p_k \\ \text{in link } i \\ \text{at time } t}} m. \tag{3}$$

The displacement pdf $g(\boldsymbol{X}, t)$ of each parcel is established based on the dynamics of sand transport. A pathway $\gamma_i=\{\xi_i, \ldots, \xi_\Omega\}$ that a parcel introduced into link i will follow before reaching the basin outlet Ω is defined as the set of geomorphic states from ξ_i (short-hand notation for $\xi_{f,i}$) through the network to the outlet (i.e., $\xi_i \rightarrow \ldots \rightarrow \xi_\Omega$). The time t_i a parcel spends in geomorphic state ξ_i can equally well be thought of as a travel time through, or residence time within, geomorphic state ξ_i. The travel time t_i is a random variable which can be described by the pdf $f_{\xi_i}(t)$ that embodies the dynamics (and inherent variability) of sand transport. In the formulation considered herein, the travel time t_i is described deterministically following the derivation presented by *Czuba and Foufoula-Georgiou* [2014] based on an elaborate analysis of sand transport assuming: (1) uniform (normal) flow, (2) that *Engelund and Hansen's* [1967] sediment-transport formula represents the sand-transport process (neglecting the shear stress partition for bedforms), (3) hydraulic geometry scaling of streamflow depth, width, and velocity, (4) an intermittency of flows that transport the majority of sediment, (5) that sediment supply does not exceed transport capacity, and (6) that sediment does not enter long-term floodplain storage. An overview schematic of this formulation is presented in Figure 2. See *Czuba and Foufoula-Georgiou* [2014] for a detailed discussion of the formulation and its limitations.

Under this formulation, the travel time t_i of a sand parcel p_k in a geomorphic fluvial state $\xi_{f,i}$ was computed as the time it takes a sand parcel to move through a link of length ℓ_i at a bulk sand transport velocity $u_{s,i}$ (LT^{-1}) as

$$t_i=\frac{\ell_i}{u_{s,i}}. \tag{4}$$

The bulk sand transport velocity $u_{s,i}$ was obtained by decomposing the volumetric transport rate of sand $Q_{s,i}$ ($\mathrm{L}^3\mathrm{T}^{-1}$) into a velocity and two length scales as

$$Q_{s,i}=u_{s,i}(\theta H_i)B_i, \tag{5}$$

where H_i (L) is the channel depth of link i, B_i (L) is the channel width of link i, and θ is a scale factor such that together (θH_i) defines a characteristic vertical length scale for sand transport where the majority of sand transport takes place. After combining equations for channel hydraulics, sand transport, and

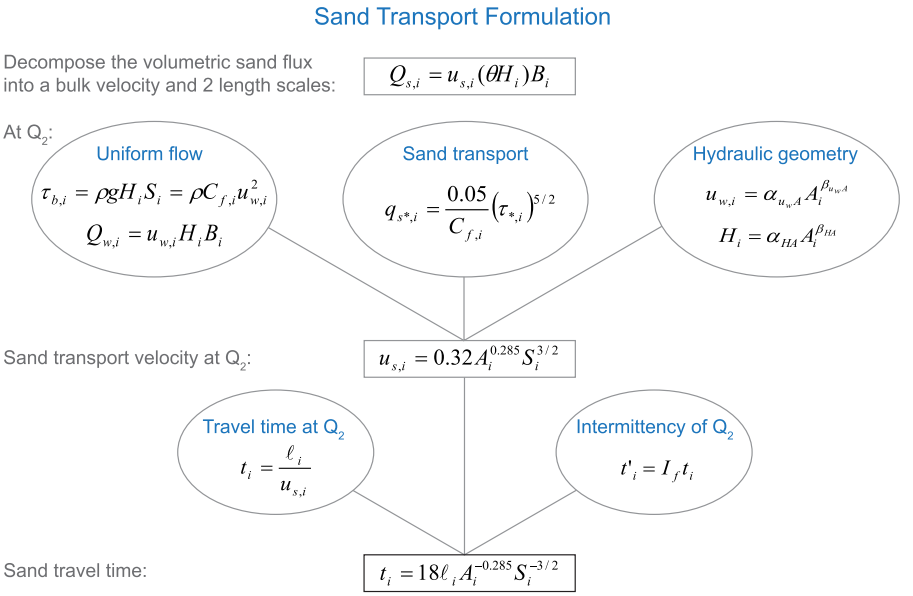

Figure 2. Overview of the formulation of sand travel time (t_i) through a fluvial geomorphic state (here link *i*, with its geomorphic and hydraulic properties). The reduced form of the sand transport velocity and sand travel time incorporates parameters specific to the Blue Earth River Basin. The characteristic flow considered in these computations is the 2 year recurrence interval peak flow or Q_2. See text for definitions.

volumetric transport rate of sand (see Figure 2 and *Czuba and Foufoula-Georgiou* [2014]), the bulk sand transport velocity is given as

$$u_{s,i} = \frac{0.05}{\theta g^{1/2} R_i^2 D_i} u_{w,i}^2 H_i^{1/2} S_i^{3/2}, \tag{6}$$

where g (LT^{-2}) is the acceleration due to gravity, R_i is the submerged specific gravity of sediment in link *i*, D_i (L) is the sediment grain size in link *i*, and $u_{w,i}$ (LT^{-1}) is the streamflow velocity of link *i*. By further incorporating hydraulic geometry relations that parameterize $u_{w,i}$ and H_i as functions of upstream drainage area A_i at a characteristic flow, accounting for an intermittency of flows I_f that transport the majority of sediment based on that characteristic flow [*Paola et al.*, 1992; *Parker*, 2004], and substituting equation (6) into equation (4), the travel time t_i of a sand parcel p_k in a geomorphic fluvial state $\xi_{f,i}$ can be obtained as

$$t_i = \frac{\theta g^{1/2} R_i^2 D_i}{0.05 \alpha_{u_wA}^2 \alpha_{HA}^{1/2} I_f} \ell_i A_i^{-(2\beta_{u_wA} + \beta_{HA}/2)} S_i^{-3/2}, \tag{7}$$

where α_{u_wA} and α_{HA} are empirically derived coefficients and β_{u_wA}, and β_{HA} are empirically derived exponents of the hydraulic geometry scaling relations.

Sand-transport dynamics have been reduced to physically based time delays in a way that greatly simplifies the flux computation such that each sand parcel p_k moves through a geomorphic fluvial state $\xi_{f,i}$ with a travel time t_i. After a parcel spends t_i amount of time in geomorphic fluvial state $\xi_{f,i}$, it transitions to the immediately downstream link where it spends some amount of time before transitioning again. When considering long-term storage in an adjacent floodplain geomorphic state, there may be a probability of first entering into long-term floodplain storage before returning back to the fluvial channel and then on to the downstream link. But in this formulation, by neglecting long-term floodplain storage of sand and only considering transport below capacity, the travel time t_i of a sand parcel in a geomorphic fluvial state $\xi_{f,i}$ represents a lower bound on the fastest time scale for sand to transport through the system.

In the network context, the travel time T_i along pathway γ_i is the sum of travel times through each of the geomorphic states comprising the pathway as $T_i = t_i + \ldots + t_\Omega$. In theoretical formulations, the travel times $\{t_i + \ldots + t_\Omega\}$ are often considered independent random variables such that the derived distribution $f_{\gamma_i}(t)$ of the sum of the travel times $\{t_i + \ldots + t_\Omega\}$ can be written as the convolution of the individual travel time pdfs as $f_{\gamma_i}(t) = f_{\xi_i} * \ldots * f_{\xi_\Omega}$. Herein, we do not seek analytical solutions as the physical properties of every link are explicitly considered and are too complex to be described analytically.

Within this transport formulation, it is relatively simple to incorporate functional dependencies between attributes of a geomorphic state ξ_i and attributes of a parcel p_k traveling in link i, as well as the accumulation of mass $m_i(t)$ in that link i due to the transport of other parcels. For instance, the transport of coarse sediment through a fluvial channel depends on the slope of the channel which depends on the accumulation of sediment in the channel (i.e., mass of all parcels in a link) which circles back to affect the slope of the channel. Additionally, an excessive accumulation of sediment in a link or high streamflow (when considering both water and sediment fluxes simultaneously) may be used to signal the input of more sediment to the network through a bank-erosion mechanism. Each of these variables can be updated in our framework at any time t depending on the state of any of the other variables. Thus, this transport formulation can couple geomorphic properties with density-dependent transport together with autogenic inputs, all within a network context.

2.3. Dynamic Connectivity

We are interested in quantifying the "dynamic connectivity" of these parcels as they are organized on the network and how this connectivity changes over time. Specifically, we are interested in defining "clusters" describing where mass coalesces into a connected extent of the network at a given time t. Within the proposed transport formulation which tracks individual parcels over links of the network, clusters can be defined in two ways: (1) using links as the elementary distance unit or (2) using the actual distance between adjacent parcels as the distance unit.

1. Link definition: this definition is based on assigning the mass m of a parcel to the link within which the parcel trajectory $\boldsymbol{X}(t)$ at time t falls. Two adjacent links are considered connected at time t if both links have at least one parcel in them. Then a cluster is defined as the set of consecutively connected links (Figures 1e and 1f). This definition can be modified by changing the mass threshold to more than one parcel per link depending on the problem at hand.

2. Interparcel distance definition: two situations can arise using the link definition that one might want to avoid: (1) the presence of one parcel in a very long link at time t that augments a cluster or (2) the absence of parcels in a very short link at time t that breaks up a cluster. Both of these situations arise due to the variable discreteness of the measuring unit (link length). Therefore, we apply a continuous distance measure which is the actual distance between adjacent parcel p_k and p_l computed along the network, i.e.,

$$d_{k,l}(t) = \left| \boldsymbol{X}_{p_k}(t) - \boldsymbol{X}_{p_l}(t) \right|_{\substack{Along \\ Network}}, \tag{8}$$

   called the inter-parcel distance $d_{k,l}(t)$ (L). Then by selecting a threshold distance d^* (L), we define a cluster by considering the set of all adjacent parcels (upstream and immediately downstream parcels along the network) whose inter-parcel distances $d_{k,l}(t)$ are $\leq d^*, \forall p_k, p_l$ parcels within the cluster (Figures 1g and 1h).

Although we have implemented both definitions, herein we only report clusters defined by the inter-parcel distance definition and denote $C_j(t)$ as the cluster j that at time t was composed of the set of parcels with inter-parcel distances of at most d^* (a procedure to compute d^* is discussed later). Once a cluster has been defined, we compute its total mass $M_j(t)$ (M) as the sum of all parcel masses within the cluster, i.e.,

$$M_j(t) = \sum_{\substack{\text{parcels } p_k, p_l \\ \text{in cluster } j \\ \text{at time } t}} m, \qquad \text{s.t.} \quad d_{k,l}(t) \leq d^*, \tag{9}$$

and its total length $L_j(t)$ (L) as the sum of (upstream and immediately downstream along the network) inter-parcel distances, i.e.,

$$L_j(t) = \sum_{\substack{\text{parcels } p_k, p_l \\ \text{in cluster } j \\ \text{at time } t}} d_{k,l}(t), \qquad \text{s.t.} \quad d_{k,l}(t) \leq d^*. \tag{10}$$

At any time t, many distinct clusters within the network may exist forming a set of clusters, each with its own properties of mass and length. From the perspective of a link, clusters form, grow, move by, or break apart through time. The hypothesis is that locations where sediment accumulates (forming clusters of a length exceeding several link lengths) and persists for a considerable period of time are more prone to fluvial geomorphic change, and thus may potentially identify hotspots of fluvial geomorphic change. To test

this hypothesis, we define a "cluster persistence index" (CPI) or CPI_i (MT) (to denote a specific value of the index for link i) which considers on every link i the cumulative effects of all clusters j that have occupied that link from time $t = 0$ until all parcels have left the system as

$$CPI_i = \int_{\substack{\text{over all}\\ \text{times } t}} M_j^{(i)}(t)\ dt, \tag{11}$$

where the superscript (i) denotes all clusters $M_j^{(i)}(t)$ that occupy link i at time t. Because the spatial extent of clusters is defined continuously on the network (i.e., using the inter-parcel distance definition and not the discrete link definition), the cluster persistence index can also be defined continuously on the network, although here we only evaluate the CPI_i at each link i.

The CPI is analogous to an impulse from classical mechanics, where an impulse is the integral of a force over time (with units of force $\times$ time) representing the change in linear momentum over that time. Instead of the integral of a force, the CPI is the integral of the mass of any cluster spanning link i over all times (with units of mass $\times$ time) representing the persistence of mass over time. In this way, the CPI identifies areas where mass has a tendency to persist that may induce sediment-driven fluvial geomorphic change. It is important to note that the CPI is not directly related to geomorphic work or stream power. Power is the rate of doing work (with units of force $\times$ velocity) and within the context of stream power is $\rho g Q_{w,i} S_i$ [e.g., see *Leopold et al*., 1964]. Stream power then is the rate of energy dissipation against the stream bed or banks by the flowing water per unit downstream length. Hotspots of streamflow-driven fluvial geomorphic change can be identified by stream power or bed shear stress ($\tau_{b,i} = \rho g H_i S_i$ ($ML^{-1}T^{-2}$)), whereas hotspots of sediment-driven fluvial geomorphic change can be identified by the persistence of sediment through the CPI_i. The longer sediment persists in a reach, the more likely it is that sediment accretion on point bars is forcing erosion of the outer bank, leading to channel migration through the so-called bar-push mechanism.

3. Application to the Greater Blue Earth River Basin

The dynamic connectivity framework was applied to sand transport on the Greater Blue Earth River Network. Section 3.1 includes a history of the basin, presenting the motivation for identifying potential hotspots of fluvial geomorphic change. Then in applying the framework, section 3.2 includes a description of the fluvial channel network and the parameterization of the travel-time formulation for sand transport. Finally, section 3.3 includes a description of sand transport on the river network, and quantification of the dynamic connectivity and the emergence of clusters of sand.

3.1. Landscape History

The Greater Blue Earth River Basin, which comprises the Watonwan, Blue Earth, and Le Sueur River Basins, drains about 9,200 km^2 of Minnesota and Iowa and is a tributary to the Minnesota River (Figures 3a and 3b). This basin has been sculpted by glaciers and post glacial processes, with two notable geomorphic processes [see *Gran et al*., 2013]. The first occurred during glacial retreat with the formation of a proglacial lake known as Glacial Lake Minnesota [*Ojakangas and Matsch*, 1982], which covered a portion of the Greater Blue Earth Basin (Figures 3c and 3d; the approximate historical extent of historical Glacial Lake Minnesota was determined as the extent of the glaciolacustrine environment by *Hobbs and Goebel* [1982]). The second began around 13,400 years ago with the carving of the Minnesota River valley after Glacial Lake Agassiz drained catastrophically through the proto-Minnesota River [*Clayton and Moran*, 1982]. This event lowered the base level of the Greater Blue Earth River creating a knickpoint, or sharp increase in channel gradient, at the mouth of the river. Over time, this knickpoint has migrated 35–40 km upstream creating a knickzone (extent shown as 40 km from the basin outlet in Figures 3d and 3f) of rapidly incising channels disconnected from their floodplains [*Gran et al*., 2009, 2011b, 2013; *Belmont*, 2011; *Belmont et al*., 2011]. Upstream of the knickzone, streams meander through low-gradient uplands (Figures 3d and 3f) that were historically dotted with poorly drained wetlands [*Marschner*, 1974].

Throughout the basin, wetlands were drained beginning in the late 1800s for agriculture. The construction of surface ditches and installation of subsurface drain tiles continued as agriculture expanded throughout the basin. As of 2011, agriculture accounted for 85% of the land use in the basin [*Jin et al*., 2013]. While an

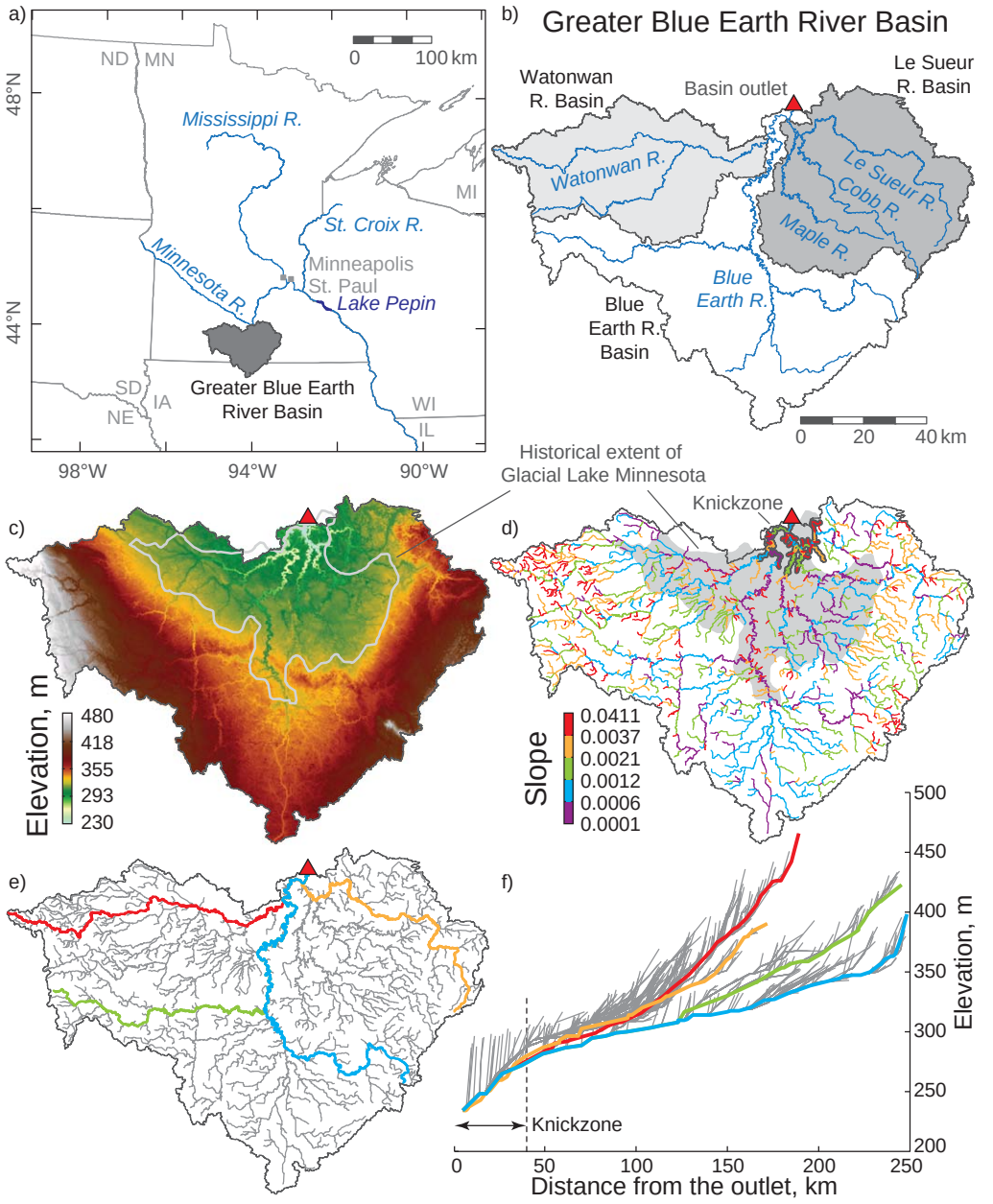

Figure 3. Location and description of the Greater Blue Earth River Network. (a) Location map of the Greater Blue Earth River Basin in Minnesota and Iowa comprising the (b) Watonwan, Blue Earth, and Le Sueur River Basins. (c) Elevation map of the basin and (d) slopes of the network. The approximate historical extent of Glacial Lake Minnesota (determined as the extent of the glaciolacustrine environment by *Hobbs and Goebel* [1982]) is shown as a light gray line in Figure 3c and a shaded gray area in Figure 3d. The knickzone in the lower 40 km of the network from the basin outlet is identified in Figure 3d as a dark gray highlighted portion of the network. (e) Traces along the network shown as (f) long profiles. The gray lines show the long profile for every link in the network to the outlet and a few traces are highlighted in color.

extensive subsurface drainage system has reduced erosion from upland fields, a consequence was the creation of more erosive rivers and an increase in sediment erosion from near-channel sources such as banks and bluffs [*Belmont et al*., 2011; *Schottler et al*., 2014]. The Greater Blue Earth River Basin has historically exported a disproportionally large amount of sediment compared to surrounding basins [*Kelley and Nater*, 2000], and as of 2002–2006 contributed over 50% of the sediment supply to the Minnesota River despite only accounting for roughly 20% of the total area [*Wilcock*, 2009]. Since European settlement, sediment export from this basin has skyrocketed, increasing by over an order of magnitude in just over a century

[*Kelley and Nater*, 2000]. While near-channel sources of sediment have been identified as the culprit [*Belmont et al*., 2011], management actions require an identification of hotspots to prioritize management actions [*Gran et al*., 2011a].

3.2. Network Extraction and Sand Transport Formulation

Applying the dynamic connectivity framework to this basin first requires extracting the river network. The Greater Blue Earth River Network was obtained from the National Hydrography Dataset Plus Version 2 (NHDPlusV2) [*McKay et al*., 2012; *Horizon Systems*, 2014]. The process of converting the NHDPlusV2 network into a useable network for this analysis included clipping the NHDPlusV2 network to the basin extent, removing isolated and secondary channels, and establishing a new set of links, with one link between tributary junctions, and with attributes mapped or recomputed for the extent of the new link from the original NHDPlusV2 network. This process created a new network derived from the NHDPlusV2 network (Figure 3) with each link connecting to 1 downstream link and either 0 or 2 upstream links, and with attributes: index of link i, index of downstream link, link length ℓ_i, upstream drainage area A_i, elevation of upstream and downstream ends of each link, and channel slope S_i (note all slopes less than 0.0001 were set to this value). Link lengths for this Greater Blue Earth River Network varied from 30 m to 25 km (mean = 4 km, median = 3 km, with an exponential distribution). Every link in this network was treated as a fluvial channel (i.e., geomorphic fluvial state) and all attributes of the geomorphic fluvial state were treated as constant in time.

Next, the travel time t_i of a sand parcel p_k in a geomorphic fluvial state $\xi_{f,i}$ was reduced to a function of only network properties by assigning parameters specific to the Greater Blue Earth River Basin. These parameters included: $g = 9.81$ m·s^{-2}, $\theta = 0.1$, $R_i = 1.65$ ($\forall i$), $D_i = 0.0004$ m ($\forall i$; D50 size of sand from riverbed material [*U.S. Geological Survey*, 2014]), $\alpha_{u_w,A} = 0.20$, $\beta_{u_w,A} = 0.07$, $\alpha_{HA} = 0.0029$, $\beta_{HA} = 0.29$ (computed at the 2 year recurrence interval peak flow Q_2 and using streamflow and channel cross-sectional properties of 23 stations; here A_i is specified in m^2, H_i in m, and $u_{w,i}$ in m·s^{-1}), and $I_f = 0.175$ (computed from a flow-duration curve; see Appendix A and B of *Czuba and Foufoula-Georgiou* [2014] for details). Substituting these parameters into equation (6) reduces the bulk sand transport velocity $u_{s,i}$ to

$$u_{s,i} = 0.32 A_i^{0.285} S_i^{3/2}, \tag{12}$$

where $u_{s,i}$ is given in meters per second. Similarly, substituting these parameters into equation (7) reduces the travel time t_i of a sand parcel p_k in a geomorphic fluvial state $\xi_{f,i}$ to

$$t_i = 18 \ell_i A_i^{-0.285} S_i^{-3/2}, \tag{13}$$

where ℓ_i is specified in meters and thus t_i is given in seconds (Figure 2).

Using equation (13) to specify how a parcel moves through each link of the network, the locations of sand parcels were then computed at a time step of about 23 days (which arose by using a time step of 4 days for transport at a constant Q_2 and accounting for the intermittency factor of 0.175) such that several time steps were required before most parcels moved through each link of the network. The time step here merely serves as the discrete time interval at which the parcel locations are being "viewed" during the continuous parcel transport through the network. This time step does not affect how parcels are transported in any way because there are no feedbacks among the number of parcels in a link, parcel transport, and the attributes of the fluvial geomorphic state in this application.

3.3. Dynamic Connectivity and Emergent Clusters of Sand

An instantaneous spatially uniform input (at time $t = 0$) of sand parcels, each representing a hillslope contribution, was "organized" by the river network structure and process dynamics into a spatially heterogeneous distribution on the network as time evolved (Figure 4). Early on ($t = 0.4$ years), sand parcels were distributed throughout the basin and over time ($t = 4$ years) sand concentrated in downstream channels. Eventually (by $t = 40$ years), sand concentrated in the main stem channels and remained there for some time before all inputs left the basin.

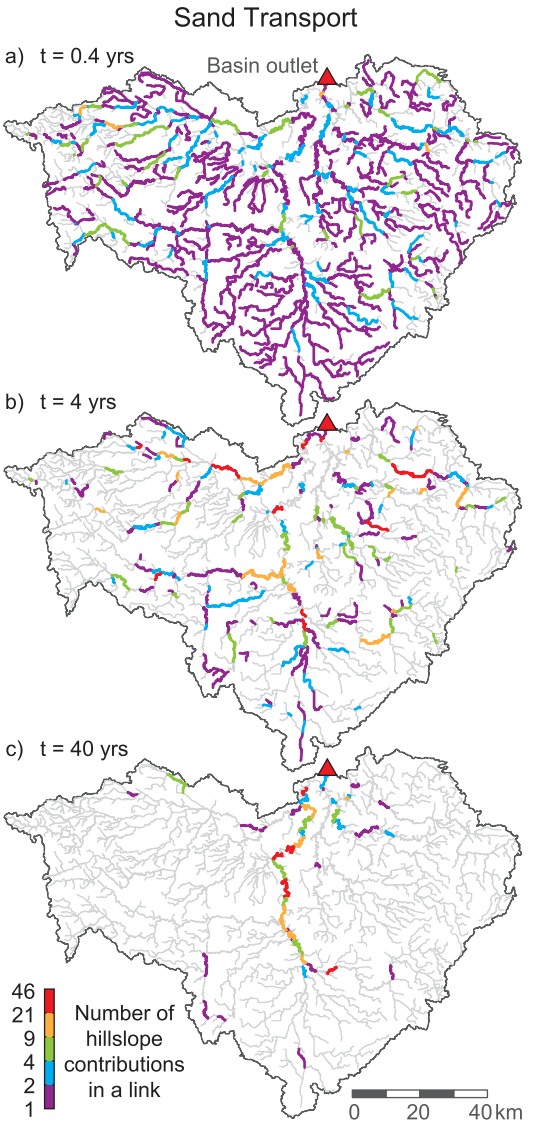

Figure 4. Sand transport on the Greater Blue Earth River Network. Organization of sand transported on the network at time (a) 0.4, (b) 4, and (c) 40 years after an instantaneous uniform input (each considered as a hillslope contribution) to all links of the network at $t = 0$.

The arrival time distribution of sand at the outlet of the basin is the sand response function (Figure 5c; see *Czuba and Foufoula-Georgiou* [2014]). The sand response function captures the combined network structure and process dynamics through time delays of sand transport on the network. This is in contrast to the network width function (Figure 5a), which captures the distance distribution of each link of the network to the outlet. Sand transport dynamics embodied by equation (13), rearrange, and reorder hillslope contributions compared to uniform velocity transport on the network (given by the network width function). This effect was not only apparent in the redistribution of mass in the sand response function compared to the width function, but also in the spatial distribution of contributions to the outlet where more mass arrived sooner than the distance alone would explain (Figure 5). This speaks for the nonlinear "stretching" of distance to time arising from the process dynamics on the river network. It also highlights the process-dependent nature of the "coarse-graining" of the landscape, i.e., partitioning the basin in spatial units that contribute almost simultaneously to the outlet. Furthermore, the sand response function illustrates the complex response of sediment yield at the outlet of a basin to a disturbance event, even under uniform input and simplified process dynamics, in accordance with other modeling literature [e.g., *Wainwright*, 2006].

Internally within the network before all sand arrived at the outlet, the location of each parcel was tracked through time and the inter-parcel distance $d_{k,l}(t)$ between every parcel and its nearest downstream parcel was measured for all times. This captured the nearest upstream and downstream inter-parcel distances between all parcels in the system at all times. At each time step, the pdf of inter-parcel distance was obtained and is plotted in Figures 6a–6d. In these figures, the pdfs were rescaled by setting their modes to one to allow a better visual representation of their time evolution (modes were assigned the same color). An interesting abrupt shift in the mode of the pdfs of inter-parcel distance (loosely referred to as a "phase transition") was observed. This phase transition occurred around 0.4 years and shifted the most probable inter-parcel distance from about 4 km when parcels were relatively far apart to about 100 m when parcels came close to each other by around 4 years (see Figures 6a–6d, where the vertical lines correspond to 0.4, 4, and 40 years). These two length scales of inter-parcel distance (4 km and 100 m) emerged from the process dynamics on the hierarchical branching network: the 4 km length scale arose from a characteristic scale of link lengths (4 km is the mean of the link length distribution), and the 100 m length scale arose from system dynamics positioning parcels close together over time. Based on the separation of these two length scales of inter-parcel distance, we set a distance threshold of $d^* = 1$ km

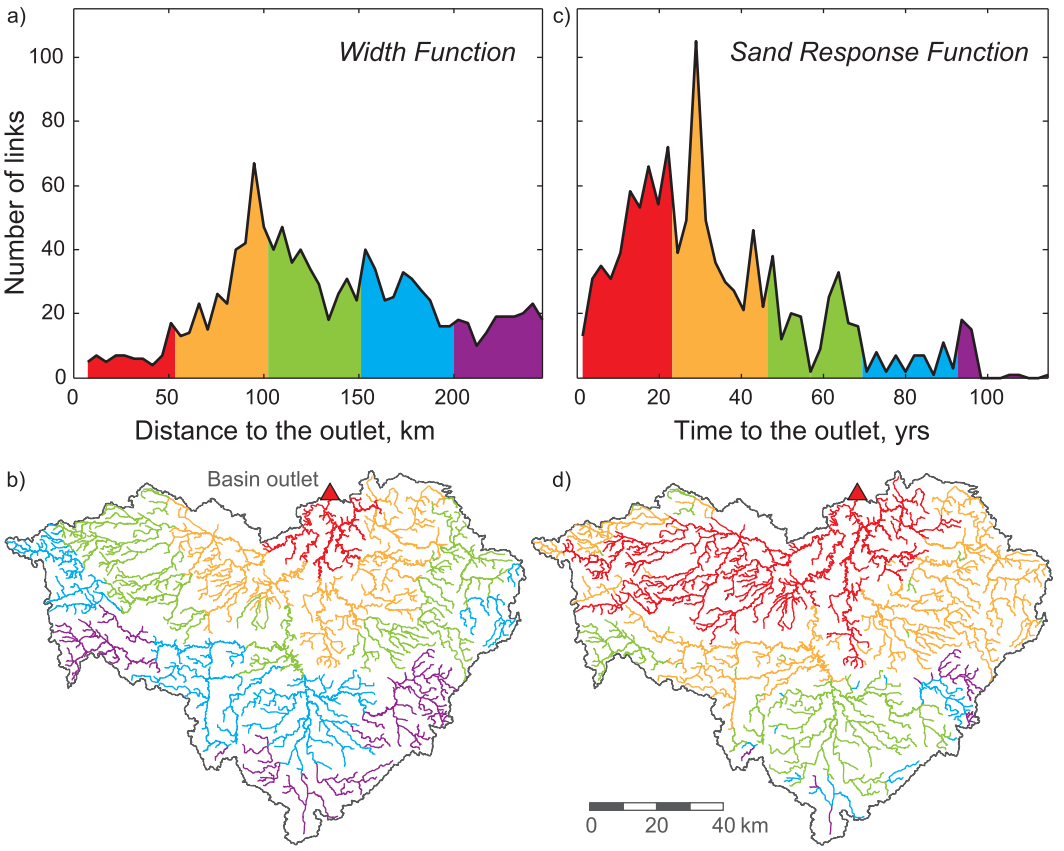

Figure 5. Distance and travel time distributions of each link to the outlet in the Greater Blue Earth River Network. The distance distribution of each link to the outlet was partitioned into different distance bands shown as (a) the network width function and (b) mapped spatially on the network. The travel time distribution of each link to the outlet was partitioned into different travel time bands shown as (c) the sand response function and (d) mapped spatially on the network. Colors correspond between Figure 5a and 5b and separately for Figure 5c and 5d.

(long-dashed horizontal line, Figure 6d) for defining a cluster. By setting this distance threshold, clusters only form when the system dynamics bring parcels within close proximity. The evolution of all clusters was then tracked over time throughout the river network. At each time step, there was a distribution of cluster sizes. Specifically, the number of clusters and a few statistics describing spatial cluster size (maximum, 90th percentile, and median) are shown in Figures 6e and 6f.

Early on (before $t = 0.4$ years), small clusters formed as parcels were transported to downstream links. The number of clusters achieved a maximum around 0.4 years, just before the beginning of the phase transition of inter-parcel distance (Figure 6). During this time, clusters were spread throughout the branches of the network (Figure 7a), while over time parcels transported farther downstream forming larger and fewer clusters. The maximum spatial cluster size formed around 4 years, after the phase transition of inter-parcel distance (Figure 6). At this time, clusters were more concentrated in downstream channels but could still be found throughout the basin (Figure 7b).

Multiple peaks of the maximum spatial cluster size occurred through time (Figure 6f). The first major peak around 4 years (see Figure 7b) and the second around 10 years were both concentrated in the same location along the Watonwan River. These multiple peaks corresponded to hillslope contributions from two different source areas each coalescing into a large cluster at this location before moving through the system. The third major peak of the maximum spatial cluster size occurred around 40 years (Figure 6f) and corresponded to a reach of the Blue Earth River (Figure 7c). Note the large temporal fluctuations of the (short-lived) max cluster size and the more robust in time 90th percentile and median cluster sizes. Our CPI is by definition highest when both a large size cluster exists and also has a long temporal persistence at the same location, as this increases the potential for sediment-driven fluvial geomorphic change. Eventually,

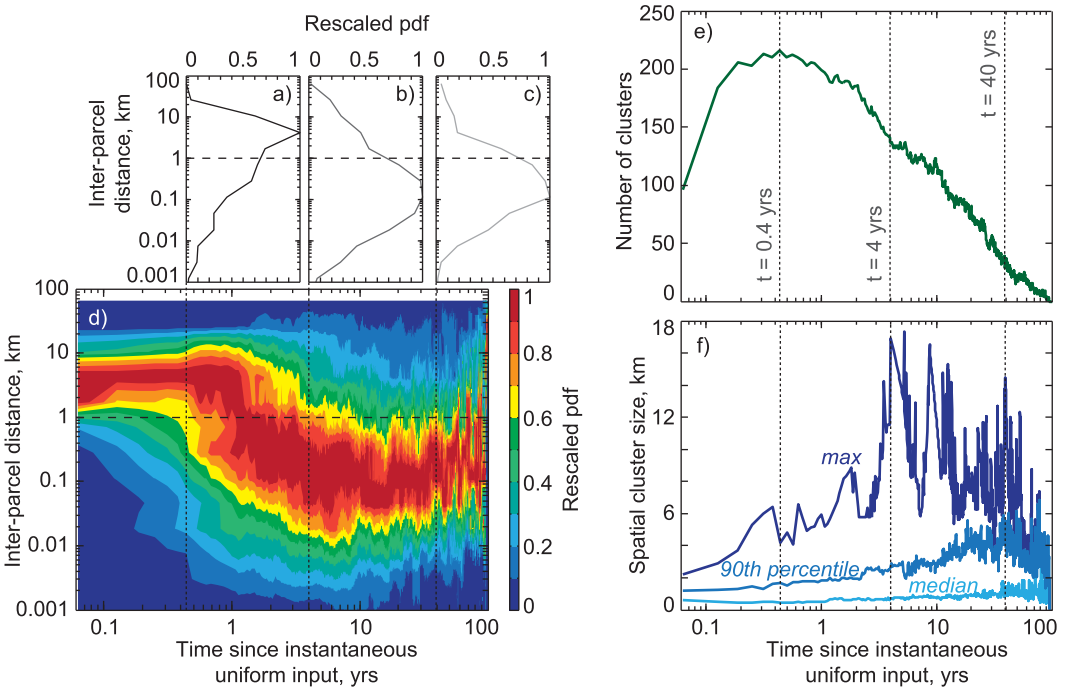

Figure 6. Temporal evolution of interparcel distance (distance between a parcel and its immediately downstream parcel) and cluster statistics. The rescaled probability distribution function (pdf) of interparcel distance (rescaled such that the mode of the pdf was set equal to 1) at time (a) 0.4, (b) 4, and (c) 40 years after an instantaneous uniform input at $t = 0$ to all links of the network. (d) Stacked pdfs of rescaled interparcel distance for all times to form a contour plot. The long-dashed horizontal line denotes the threshold distance (d^*) used in the (interparcel distance) cluster definition, i.e., two parcels less than d^* distance apart belong to the same cluster. (e) Number of clusters formed over time and (f) cluster size statistics of maximum, 90th percentile, and median spatial cluster size.

the cluster size statistics go to zero as all the sand parcels leave the system. A movie showing the temporal evolution of sediment propagation and clustering for all time steps (including the three snapshots of Figure 7) is included as supporting information Movie S1.

4. Identifying Hotspots of Fluvial Geomorphic Change

The question posed here is whether, within the dynamic connectivity framework, the emergence of sediment clusters that are integrated through time into the CPI can be used as a tool for (a) identifying hotspots of fluvial geomorphic change and (b) gaining insight into the possible driving mechanisms of this change. In our basin, we used channel migration as a measure of fluvial geomorphic change and specifically focused on three places within the basin where high rates of channel migration have been observed (defined as hotspots). Channel migration data were measured within 20 m increments for the downstream portions of the Watonwan, Blue Earth, Maple, and Le Sueur Rivers by comparing the movement of digitized river channels from two sets of aerial photographs from 1938 and 2005 to provide an average migration rate over the time period 1938–2005 (Figure 8a; all channel migration data shown have been spatially averaged using a 5 km smoothing window) [*Belmont et al.*, 2011; *Bevis*, 2014]. The spatial pattern of channel migration was heterogeneously distributed on the river network, with three specific reaches of high rates of change (here denoted as h1, h2, and h3) along the Watonwan (h1), Blue Earth (h2), and Le Sueur (h3) Rivers (Figure 8a).

The CPI (equation (11)) integrates the evolution of clusters in the Greater Blue Earth River Network following an instantaneous spatially uniform input to all links of the network and identifies areas of the network where mass concentrates and persists due to time delays on the hierarchical branching river network structure. As discussed before, the purpose of using an instantaneous spatially uniform input was to probe the system and examine its emergent space-time organization, e.g., critical locations where inputs slow down and cluster together (as identified by high CPI), revealing a system property due to network topology and process dynamics. We seek to test the hypothesis that places of high CPI can be used to identify observed hotspots of sediment-driven channel migration. It is seen from Figure 8 that the CPI was capable of identifying hotspots

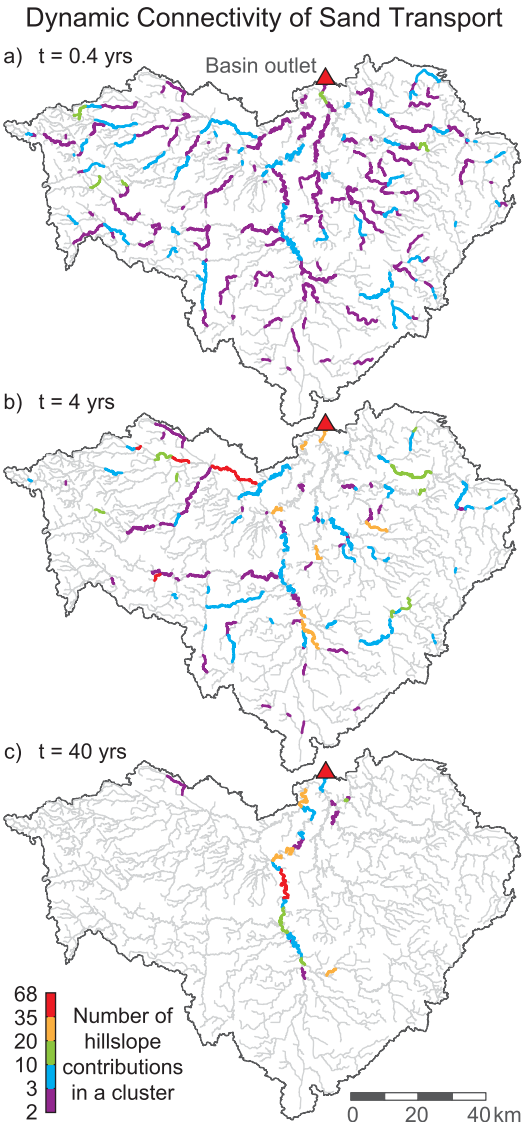

Figure 7. Dynamic connectivity of sand transport on the Greater Blue Earth River Network. Organization of sand transported on the network into clusters at time (a) 0.4, (b) 4, and (c) 40 years after an instantaneous uniform input (each considered as a hillslope contribution) to all links of the network at $t = 0$. Clusters were defined using an interparcel distance (distance between a parcel and its immediately downstream parcel) equal to 1 km although they are shown here as spanning entire links. The color corresponds to the number of hillslope contributions within each cluster. A movie showing the temporal evolution of sediment propagation and clustering for all time steps (including the three snapshots shown here) is included as supporting information Movie S1.

h1 and h2 on the Watonwan and Blue Earth Rivers, respectively, that occurred upstream of the knickzone. This might suggest that these hotspots occurred because of a persistence of sediment, forcing channel migration through the bar-push mechanism [*Parker et al.*, 2011; *van de Lageweg et al.*, 2014; *Eke et al.*, 2014].

It is noted that in making cause and effect interpretations, it is important to examine the system predisposition for geomorphic change (as performed above) in view of the possibly heterogeneous spatiotemporal inputs which might negate such a predisposition. For example, an asynchronous timing of sediment supply might ameliorate or even break down the persistence of sediment clustering, depending on the time scales of sediment pulsing versus the time scales of transport. In our case, numerical experiments by randomly varying the starting positions of parcels within the length of each link and also by increasing sediment input at locations where bluffs adjoin the river network (the major sources of accelerated sediment input in this basin), have clearly demonstrated that this is not the case, and that the locations of high CPI are fairly robust. This issue is further discussed in section 5 where unraveling the sources of clusters is proposed as a means for guiding management decisions.

As can be seen from Figure 8, the CPI qualitatively matches the observed channel migration rate upstream of the knickzone in both the Watonwan and Blue Earth Basins with one exception. At about 15 km upstream of the mouth of the Blue Earth River, CPI was very large but the observed channel migration rate was low (see Figure 8d). This is the site of Rapidan Dam on the Blue Earth River, which in the network had a very low slope, representative of the reservoir surface. Obviously the reservoir is not migrating and thus the local context must always be considered in interpreting the results of the analysis.

Hotspot h3 on the Le Sueur River that occurred within the knickzone was not identified by a high magnitude of CPI (Figure 8). This might suggest that a different mechanism, such as the streamflow-driven bank-pull mechanism [*Parker et al.*, 2011; *van de Lageweg et al.*, 2014; *Eke et al.*, 2014], was responsible for the amplified migration in hotspot h3. Indeed, the bank-pull mechanism is expected to occur in reaches with high bed shear stress capable of both eroding the channel banks and rapidly transporting supplied sediment downstream, such as in the knickzone where hotspot h3 lies. Bed shear stress $\tau_{b,i}$ was computed for the entire network as $\tau_{b,i} = \rho g H_i S_i$ (where $\rho = 1000$ kg·m^{-3}) and is shown in Figure 9a; the area with the highest bed shear stress corresponded to hotspot h3 on the Le Sueur River, providing support for the idea that streamflow-driven erosion rather than sediment persistence may drive channel migration here. Bed

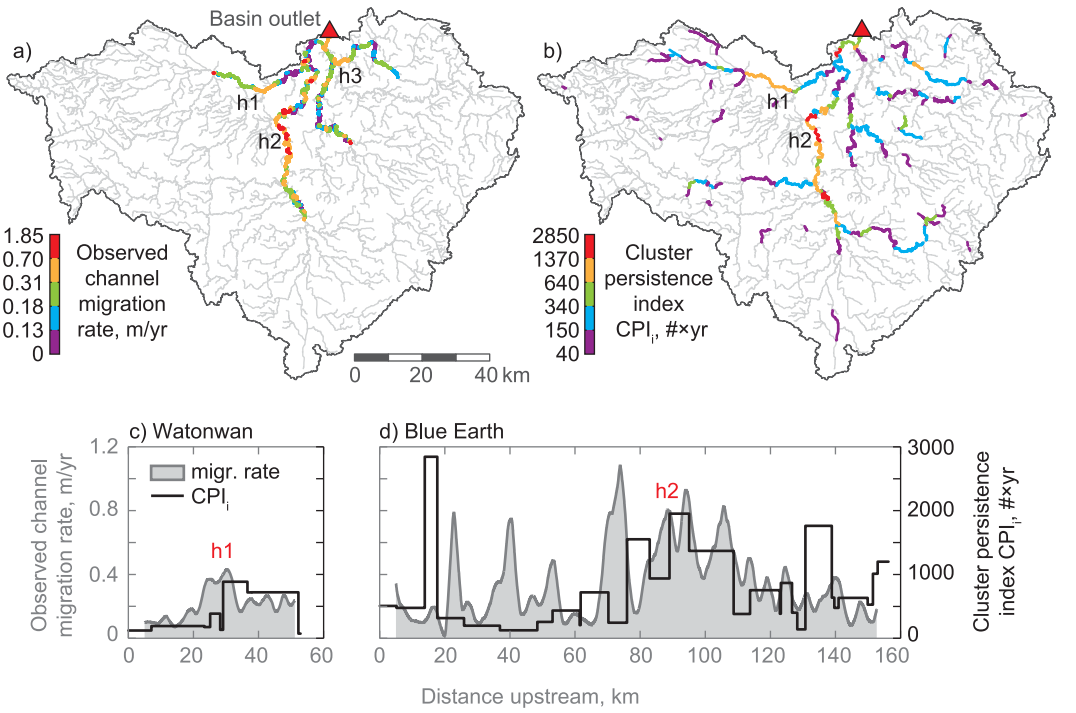

Figure 8. Identification of hotspots of fluvial geomorphic change in the Greater Blue Earth River Network using the cluster persistence index (CPI). (a) Observed channel migration rate 1938–2005 shown spatially averaged using a 5 km smoothing window [*Belmont et al.*, 2011; *Bevis*, 2014]. Hotspots (h1, h2, h3) of fluvial geomorphic change were defined as locations where the observed channel migration rate was much higher than was occurring throughout the rest of the basin. (b) CPI as computed by our model (see text for definition). High values of CPI coincide with hotspots h1 and h2 suggesting that CPI can be used to identify these hotspots of sediment-driven fluvial geomorphic change. Hotspot h3 (streamflow-driven) was not identified by CPI and reasons are discussed in the text (see also Figure 9). Detailed comparisons of the observed channel migration rate (shaded gray; corresponds to the left *y* axis) and cluster persistence index (black line; corresponds to the right *y* axis) for the (c) Watonwan River which contains hotspot h1 and (d) Blue Earth River which contains hotspot h2.

shear stress was low at hotspots h1 and h2 on the Watonwan and Blue Earth Rivers, respectively, corroborating the hypothesis that channel migration here is driven by a different mechanism than streamflow-driven erosion.

Further support for the bank-pull mechanism in contributing to the geomorphic change associated with hotspot h3 was provided by the finding that incision of this portion of the Le Sueur River over the Holocene was most accurately modeled as a detachment-limited (or supply-limited) system in which downstream coarsening also played a role in setting the modern longitudinal profile [*Gran et al.*, 2013]. Additionally, detailed measurements and field observations of eroding bluffs in this portion of the Le Sueur River suggest that undercutting and toe erosion drive bluff retreat, i.e., channel migration into bluffs, and because these bluffs maintain steep faces and do not lie back over time suggests that the river quickly removes any material deposited at the toe of the bluff [*Day et al.*, 2013]. Together these observations suggest that this portion of the Le Sueur River is more than capable of transporting any sediment supplied downstream without allowing sediment to persist for a long period of time. Therefore, in this reach of the Le Sueur River (around hotspot h3), the most likely mechanism of channel migration is the bank-pull mechanism. It is also known that in the knickzone of the Le Sueur River, large bluffs contribute a substantial amount of sediment to the river network [*Belmont et al.*, 2011] and thus it is also possible that spatiotemporal heterogeneity of sediment supply, which was not considered herein, may also play a large role in forming this hotspot. Further investigation into all hotspots is necessary to provide more evidence for the causative mechanisms leading to the observed high rates of channel migration.

Geomorphic disturbances can be amplified at and just downstream of confluences due to the high frequency and magnitude of sediment fluctuations from punctuated tributary inputs, and also directly upstream of confluences due to presence of a wider, low gradient reach that is more susceptible to geomorphic change (suggested by the network dynamics hypothesis of *Benda et al.* [2004a, 2004b]). However,

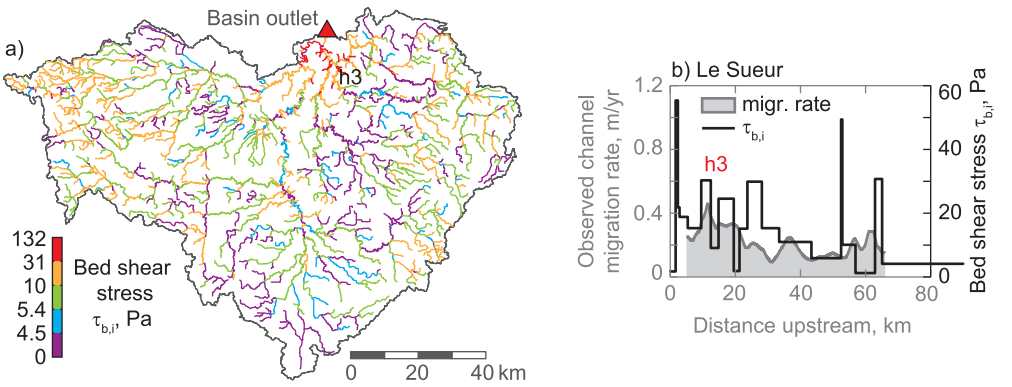

Figure 9. Identification of hotspot of fluvial geomorphic change in the Greater Blue Earth River Network using bed shear stress. (a) Bed shear stress at the 2 year recurrence interval flow. Hotspot h3 of fluvial geomorphic change was defined as the location along the Le Sueur River where the observed channel migration rate was much higher than was occurring throughout the rest of the river (see Figure 8a). It is seen that the streamflow-driven hotspot h3 was well predicted by high values of bed shear stress. (b) Detailed comparison of the observed channel migration rate (shaded gray; corresponds to the left *y* axis) and bed shear stress (black line; corresponds to the right *y* axis) for the Le Sueur River.

we caution that the potential for fluvial geomorphic change to occur farther downstream should not be overlooked. For instance, if the receiving stream is capable of transporting the sediment delivered to a confluence farther downstream, then the aggregating effects of these inputs may not manifest into fluvial geomorphic change until the transport capacity of the stream is reduced, such as at a break in slope or at a large increase in channel width. In this case, fluvial geomorphic change may not occur in direct proximity to the confluence although the merging of inputs at the confluence may be responsible for augmenting the sediment flux. This was exemplified by hotspot h2 of fluvial geomorphic change that occurred on the Blue Earth River over 14 km downstream from the nearest major confluence (Figure 8a).

We note that hotspot h2 on the Blue Earth River would not have been identified by considering confluence effects alone and that it was only identified by considering simplified process dynamics explicitly on the network. Granted, the heterogeneous distribution of slopes on the network was the primary factor leading to the identification of these hotspots. But it was not obviously apparent from a map of channel slopes (Figure 3d) specifically where hotspots of fluvial geomorphic change might arise. Only by incorporating physically based process dynamics that amplify variations in geomorphic properties, such as channel slope, through nonlinear relations within the specific hierarchical arrangement of these properties on the network, were we able to highlight critical hotspots of fluvial geomorphic change (Figure 8).

The dynamic connectivity framework provides a means for assessing potential hotspots of fluvial geomorphic change at the network scale and is ideally suited to be used as a rapid identification tool for identifying potential reaches susceptible to fluvial geomorphic change. This framework has advantages over the static spatial metrics such as channel slope (Figure 3d) or bed shear stress (Figure 9a) through which the identification of all hotspots was not readily apparent (as discussed above). To identify all potential hotpots, one should investigate both reaches of high CPI and also reaches of high bed shear stress (or high stream power, which is closely related). Then this approach can also be useful for hypothesis testing, by suggesting which mechanism of channel migration may be driving change in various locations. Once hotspots are identified using this framework, more detailed investigations can be performed at the reach scale to further understand causative mechanisms and to better inform potential management actions.

5. Unraveling the Source of a Cluster

If hotspots of fluvial geomorphic change can be identified through the emergence of large persistent clusters of mass on the network, the next question is how this information can be used to inform potential management actions. Large clusters that formed at time 4 years (corresponding to h1 on the Watonwan River, Figure 10a) and 40 years (corresponding to h2 on the Blue Earth River, Figure 10b) after an instantaneous uniform input of sand to all links of the network were unraveled backward in time to identify their source contributions (at time 0, Figure 10c). As these are the largest clusters formed, they are the clusters

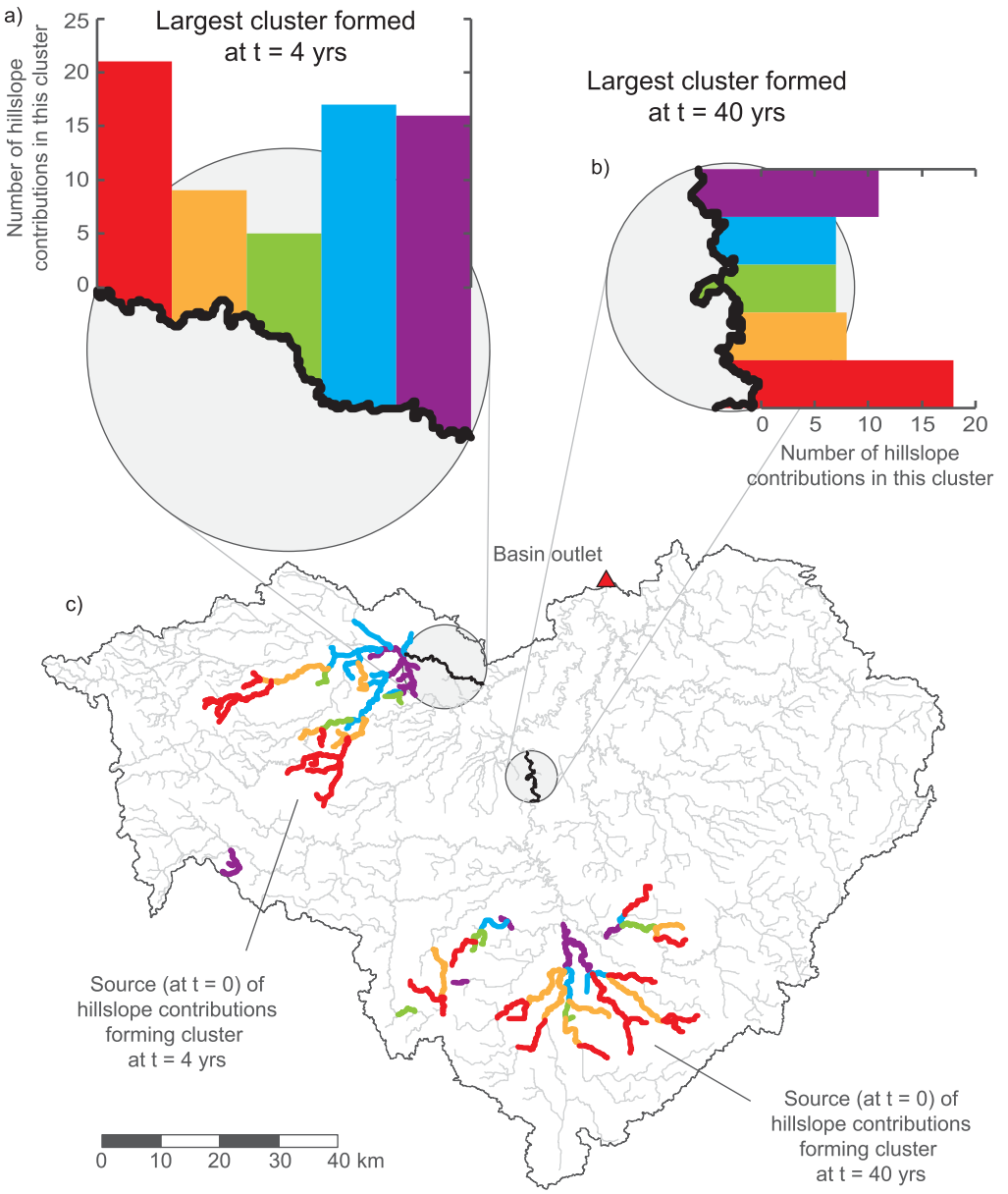

Figure 10. Unraveling the source contributions of two large clusters formed at different times. The largest cluster formed at time (a) 4 years (length ≈ 17 km) and (b) 40 years (length ≈ 15 km). The colored bars are the histogram of hillslope contributions within each cluster, where each color corresponds to a specific source area (at time 0) of the hillslope contributions composing the cluster, shown with the same colors in Figure 10c. This process-specific coarse-graining of the landscape allows the identification of space-time sources of sediment which eventually coalesce downstream due to the specific river network topology and flux dynamics.

responsible for the largest contributions to the CPI and the coalescing of their mass may most strongly exacerbate channel migration at these locations. By identifying the source contributions that synchronize on the network to form clusters, management efforts could be taken to reduce sediment generation of these specific source areas or break the synchronization of these contributions before they coalesce into an aggregated mass with a potential to affect fluvial geomorphic change.

Potential management options might include efforts to reduce the erosion at the source (through bank protection measures for bank sources or vegetative buffer strips for upland sources), break the synchronization of arrival of sediment (through construction of riparian wetlands that alter specific reach hydraulics), or mitigate the effects (through bank protection measures for the eroding bank or sediment removal where the bar-push mechanism drives erosion). Depending on the network structure and process dynamics, the potential management options available may differ.

For instance, the large cluster that formed on the Watonwan River (coincident with hotspot h1) formed early on (within 4 years of the input) and thus reflected a proximal upstream source (Figure 10). Here there was a short lead time before the cluster formed but the source areas were distributed between two branches. Efforts to break the synchronization of these inputs here before they form a cluster may be possible through alteration of the geomorphic properties affecting the travel time through one of the branches, but would likely have to be carried out prior to any disturbance due to the short lead time of cluster formation. However, we caution that any efforts to break the synchronization of a potential cluster should be fully investigated to ensure that a larger cluster would not likely form at a different time.

Alternatively, the large cluster that formed on the Blue Earth River (coincident with hotspot h2) formed later on (40 years after the input) and thus reflected a distal upstream source (Figure 10). Here there was a long lead time before the cluster formed but the source area was more scattered among several subnetworks. Multiple efforts might be required to break the synchronization of these inputs here before they form a cluster due to the distributed nature of the source area, although these efforts could be carried out after a disturbance due to the long lead time of cluster formation. Control of source inputs may be most feasible given the distributed nature of the source area because variations between different subnetworks may make source control more readily possible in some subnetworks than others.

These examples of unraveling source contributions that synchronize at a given location to affect geomorphic change are meant to be illustrative of the type of information that can come out of this framework rather than as a suggestion of where to manage to reduce channel migration in this basin. Once system specific information on spatiotemporal inputs can be considered (available from direct observations, mapping of sediment-generating landscape features, sediment budgets, etc.), then it is possible to verify whether indeed these unraveled source contributions are the main cluster-contributing sediment sources or whether these sources may be overwhelmed by larger sediment sources elsewhere in the basin.

The dynamic connectivity framework provides a network-scale context to process dynamics operating at smaller scales for informing basin management. While not a focus herein, this framework is capable of assessing how changes to the network, in either network structure or through properties such as channel width, at a local scale may cascade into larger changes at the network scale.

6. Concluding Remarks

The dynamic connectivity framework presented herein takes a network as a template upon which a flux evolves through time. We suggest that the spatial organization of fluxes into clusters can tell us something about system functioning. This framework is general enough to account for different types of networks as well as time varying properties of the system. Herein, this framework was applied to sand transport on the Greater Blue Earth River Network in Minnesota to assess the potential for using the emergence of sediment clusters, which were integrated through time into a cluster persistence index (CPI), to identify hotspots of fluvial geomorphic change. High values of CPI represent areas where sediment has a tendency to persist on the network, which may be related to sediment-driven fluvial geomorphic change. Of the three hotspots of fluvial geomorphic change (defined as locations where observed rates of channel migration were high), two of these hotspots coincided with high CPI. The third hotspot was not identified by high CPI, but instead was believed to be a hotspot of streamflow-driven change based on additional information and the fact that high bed shear stress coincided with this hotspot. Nonetheless, the dynamic connectivity framework provides a network perspective of dynamical processes that occur at smaller scales, useful for understanding how reach-scale changes cascade into network-scale effects and for informing management actions.

Notation

a_i directly contributing area to link i (L^2)
A_i upstream drainage area of link i (L^2)
B_i channel width of link i (L)
$C_{f,i}$ friction coefficient of link i

C_j	denotes the jth cluster
CPI_i	cluster persistence index of link i (MLT)
$d_{k,l}$	inter-parcel distance between parcel p_k and the nearest downstream parcel p_l (L)
d^*	inter-parcel distance threshold for defining a cluster (L)
D_i	grain size of sediment in link i (L)
$f(t)$	travel time probability distribution function at a fixed control section
$f_{\xi_i}(t)$	travel time probability distribution function through geomorphic state ξ_i
$f_{\gamma_i}(t)$	travel time probability distribution function from link i to the outlet
g	acceleration due to gravity (LT^{-2})
$g(\boldsymbol{X}, t)$	displacement probability density function
H_i	channel depth of link i (L)
i	index denoting spatial location in the network
I_f	intermittency factor for sand transport
j	index denoting a specific cluster
k	index denoting a specific parcel
l	index denoting the nearest downstream parcel of parcel p_k
ℓ_i	length of link i (L)
L_j	distance spanned by cluster C_j (L)
m_i	total mass in link i (M)
m	mass of a sediment parcel (M)
M_j	mass within cluster C_j (M)
N	total number of links in the network
p_k	denotes the kth (sediment) parcel
p_l	denotes the nearest lth (sediment) parcel downstream of parcel p_k
$q_{s*,i}$	dimensionless volumetric transport rate of sand per unit width in link i
$Q_{s,i}$	volumetric transport rate of sand in link i (L^3T^{-1})
$Q_{w,i}$	volumetric transport rate of water in link i (L^3T^{-1})
R_i	submerged specific gravity of sediment in link i
S_i	slope of link i
t_i	travel time of a sand parcel p_k in a geomorphic fluvial state $\xi_{f,i}$ (T)
t'_i	travel time of a sand parcel p_k in a geomorphic fluvial state $\xi_{f,i}$ at Q_2 (T)
t	time index
t_0	initial time index
T	arrival time of a parcel at the control section (T)
T_i	travel time from link i to the outlet (T)
$u_{s,i}$	bulk sand transport velocity of a parcel p_k through a geomorphic fluvial state $\xi_{f,i}$ (LT^{-1})
$u_{w,i}$	streamflow velocity in link i (LT^{-1})
V	arbitrary control volume
$\boldsymbol{X}$	Lagrangian coordinate of a parcel
$\boldsymbol{X}_0$	initial position of a parcel at time t_0
$\boldsymbol{X}_{p_k}$	Lagrangian coordinate of parcel p_k
$\boldsymbol{\chi}$	collection of Lagrangian parcel locations
α_{HA}	coefficient of the $H_i \sim A_i$ scaling relation
α_{u_wA}	coefficient of the $u_{w,i} \sim A_i$ scaling relation
β_{HA}	exponent of the $H_i \sim A_i$ scaling relation
β_{u_wA}	exponent of the $u_{w,i} \sim A_i$ scaling relation
γ_i	connectivity of geomorphic state ξ_i to the outlet
θ	scale factor for determining the characteristic vertical length scale for sand transport
$\xi_{f,i}$	geomorphic fluvial state of link i
ξ_i	geomorphic state of link i
ρ	density of water (ML^{-3})
$\tau_{b,i}$	bed shear stress in link i ($ML^{-1}T^{-2}$)
$\tau_{*,i}$	dimensionless bed shear stress in link i
Ω	index of the basin outlet

Acknowledgments
This research was funded by NSF grant EAR-1209402 under the Water Sustainability and Climate Program (WSC): REACH (REsilience under Accelerated CHange) and benefited from collaborations made possible by NSF grant EAR-1242458 under Science Across Virtual Institutes (SAVI): LIFE (Linked Institutions for Future Earth). Alejandro Tejedor (Univ. of Minnesota) suggested the cluster definition of inter-parcel distance be used over the link definition. We thank Patrick Belmont (Utah State Univ.), Karen Gran (Univ. of Minnesota, Duluth), and Martin Bevis (Univ. of Minnesota, Duluth) for providing the observed channel migration data. We thank two anonymous reviewers for their insightful comments which helped improve the presentation of our work, and also the Editor (Graham Sander) and Associate Editor (anonymous) for an efficient and constructive review process. A movie showing the temporal evolution of sediment propagation and clustering for all time steps (including the three snapshots of Figure 7) is included as Supporting Information (Movie S1).

References

Abad, J. D., and M. H. Garcia (2006), RVR Meander: A toolbox for re-meandering of channelized streams, *Comput. Geosci.*, *32*, 92–101, doi:10.1016/j.cageo.2005.05.006.

Alexander, K. B., et al. (2009), Dynamic modeling of nitrogen losses in river networks unravels the coupled effects of hydrological and biogeochemical processes, *Biogeochemistry*, *93*, 91–116, doi:10.1007/S10533-008-9274-8.

Belmont, P. (2011), Floodplain width adjustments in response to rapid base level fall and knickpoint migration, *Geomorphology*, *128*, 92–102, doi:10.1016/j.geomorph.2010.12.026.

Belmont, P., et al. (2011), Large shift in source of fine sediment in the Upper Mississippi River, *Environ. Sci. Technol.*, *45*, 8804–8810, doi:10.1021/es2019109.

Benda, L., and T. Dunne (1997), Stochastic forcing of sediment routing and storage in channel networks, *Water Resour. Res.*, *33*(12), 2865–2880, doi:10.1029/97WR02387.

Benda, L., N. L. Poff, D. Miller, T. Dunne, G. Reeves, G. Pess, and M. Pollock (2004a), The network dynamics hypothesis: How channel networks structure riverine habitats, *BioScience*, *54*(5), 413–427, doi:10.1641/0006-568(2004)054[0413:TNDHHC]2.0.CO;2.

Benda, L., K. Andras, D. Miller, and P. Bigelow (2004b), Confluence effects in rivers: Interactions of basin scale, network geometry, and disturbance regimes, *Water Resour. Res.*, *40*, W05402, doi:10.1029/2003WR002583.

Bertuzzo, E., S. Azaele, A. Maritan, M. Gatto, I. Rodriguez-Iturbe, and A. Rinaldo (2008), On the space-time evolution of a cholera epidemic, *Water Resour. Res.*, *44*, W01424, doi:10.1029/2007WR006211.

Bertuzzo, E., R. Muneepeerakul, H. J. Lynch, W. F. Fagan, I. Rodriguez-Iturbe, and A. Rinaldo (2009), On the geographic range of freshwater fish in river basins, *Water Resour. Res.*, *45*, W11420, doi:10.1029/2009WR007997.

Bevis, M. (2014), Pleistocene base-level fall is a fundamental driver of erosion in southern Minnesota's greater Blue Earth River basin, MS thesis, Dept. of Earth and Environ. Sci., Univ. of Minn., Duluth.

Botter, G., T. Settin, M. Marani, and A. Rinaldo (2006), A stochastic model of nitrate transport and cycling at basin scale, *Water Resour. Res.*, *42*, W04415, doi:10.1029/2005WR004599.

Bracken, L. J., J. Wainwright, G. A. Ali, D. Tetzlaff, M. W. Smith, S. M. Reaney, and A. G. Roy (2013), Concepts of hydrological connectivity: Research approaches, pathways and future agendas, *Earth Sci. Rev.*, *119*, 17–34, doi:10.1016/j.earscirev.2013.02.001.

Bracken, L. J., L. Turnbull, J. Wainwright, and P. Bogaart (2015), Sediment connectivity: A framework for understanding sediment transfer at multiple scales, *Earth Surf. Processes Landforms*, *40*(2), pp. 177–188, doi:10.1002/esp.3635.

Campbell Grant, E., W. Lowe, and W. Fagan (2007), Living in the branches: Population dynamics and ecological processes in dendritic networks, *Ecol. Lett.*, *10*, 165–175, doi:10.1111/j.1461-0248.2006.01007.x.

Carrara, F., F. Altermatt, I. Rodriguez-Iturbe, and A. Rinaldo (2012), Dendritic connectivity controls biodiversity patterns in experimental metacommunities, *Proc. Natl. Acad. Sci. U. S. A.*, *109*(15), 5761–5766, doi:10.1073/pnas.1119651109.

Ceola, S., E. Bertuzzo, G. Singer, T. J. Battin, A. Montanari, and A. Rinaldo (2014), Hydrologic controls on basin-scale distribution of benthic invertebrates, *Water Resour. Res.*, *50*, 2903–2920, doi:10.1002/2013WR015112.

Clayton, L., and S. R. Moran (1982), Chronology of late Wisconsinan glaciation in middle North America, *Quat. Sci. Rev.*, *1*, 55–82.

Czuba, J. A., and E. Foufoula-Georgiou (2014), A network-based framework for identifying potential synchronizations and amplifications of sediment delivery in river basins, *Water Resour. Res.*, *50*, 3826–3851, doi:10.1002/2013WR014227.

Day, S. S., K. B. Gran, P. Belmont, and T. Wawrzyniec (2013), Measuring bluff erosion part 2: Pairing aerial photographs and terrestrial laser scanning to create a watershed scale sediment budget, *Earth Surf. Processes Landforms*, *38*(10), 1068–1082, doi:10.1002/esp.3359.

Dust, D., and E. Wohl (2012), Conceptual model for complex river responses using an expanded Lane's relation, *Geomorphology*, *139–140*, 109–121, doi:10.1016/j.geomorph.2011.10.008.

Eke, E., G. Parker, Y. Shimizu (2014), Numerical modeling of erosional and depositional bank processes in migrating river bends with self-formed width: Morphodynamics of bar push and bank pull, *J. Geophys. Res. Earth Surf.*, *119*, 1455–1483, doi:10.1002/2013JF003020.

Engelund, F., and E. Hansen (1967), *A Monograph on Sediment Transport in Alluvial Streams*, 62 p., Tek. Forlag, Copenhagen, Denmark.

Furey, P. R., and V. K. Gupta (2007), Diagnosing peak-discharge power laws observed in rainfall-runoff events in Goodwin Creek experimental watershed, *Adv. Water Resour.*, *30*(11), 2387–2399, doi:10.1016/j.advwatres.2007.05.014.

Gran, K. B., P. Belmont, S. S. Day, C. Jennings, A. Johnson, L. Perg, and P. R. Wilcock (2009), Geomorphic evolution of the Le Sueur River, Minnesota, USA, and implications for current sediment loading, in *Management and Restoration of Fluvial Systems with Broad Historical Changes and Human Impacts*, vol. 451, edited by L. A. James, S. L. Rathburn, and G. R. Whittecar, pp. 119–130, Geol. Soc. of Am., Boulder, Colo., doi:10.1130/2009.2451(08).

Gran, K. B., P. Belmont, S. Day, C. Jennings, J. W. Lauer, E. Viparelli, P. Wilcock, and G. Parker (2011a), An integrated sediment budget for the Le Sueur River Basin, *Rep. wq-iw7-29o*, 128 p., Minn. Pollut. Control Agency, Mankato. [Available at http://www.pca.state.mn.us/index.php/view-document.html?gid=16202, last accessed 26 May 2014.]

Gran, K. B., P. Belmont, S. S. Day, N. Finnegan, C. Jennings, J. W. Lauer, and P. R. Wilcock (2011b), Landscape evolution in south-central Minnesota and the role of geomorphic history on modern erosional processes, *GSA Today*, *21*(9), 7–9, doi:10.1130/G121A.1.

Gran, K. B., N. Finnegan, A. L. Johnson, P. Belmont, C. Wittkop, and T. Rittenour (2013), Landscape evolution, valley excavation, and terrace development following abrupt postglacial base-level fall, *GSA Bull.*, *125*(11–12), 1851–1864, doi:10.1130/B30772.1.

Gupta, V. K., E. Waymire, and C. T. Wang (1980), A representation of an instantaneous unit hydrograph from geomorphology, *Water Resour. Res.*, *16*(5), 855–862, doi:10.1029/WR016i005p00855.

Gupta, V. K., E. Waymire, and I. Rodriguez-Iturbe (1986), On scales, gravity and network structure in basin runoff, in *Scale Problems in Hydrology*, edited by V. K. Gupta, I. Rodriguez-Iturbe, and E. F. Wood, pp. 159–184, D. Reidel, Dordrecht, Holland.

Gupta, V. K., R. Mantilla, B. M. Troutman, D. Dawdy, and W. F. Krajewski (2010), Generalizing a nonlinear geophysical flood theory to medium-sized river networks, *Geophys. Res. Lett.*, *37*, L11402, doi:10.1029/2009GL041540.

Heckmann, T., W. Schwanghart, and J. D. Phillips (2015), Graph theory: Recent developments of its application in geomorphology, *Geomorphology*, doi:10.1016/j.geomorph.2014.12.024, in press.

Hobbs, H. C., and J. E. Goebel (1982), *Geologic map of Minnesota, Quaternary geology*, State map series, S-1, scale 1:500,000, Minn. Geological Survey, St. Paul. [Available at http://hdl.handle.net/11299/60085, last accessed 29 May 2014].

Horizon Systems (2014), *NHDPlus Version 2*, Horizon Syst. Corp., Herndon, Va. [Available at http://www.horizon-systems.com/NHDPlus/NHDPlusV2_home.php, last accessed 20 May 2014].

Istvánovics, V., M. Honti, A. Kovács, G. Kocsis, and I. Stier (2014), Phytoplankton growth in relation to network topology: Time-averaged catchment-scale modelling in a large lowland river, *Freshwater Biol.*, *59*(9), pp. 1856–1871. doi:10.1111/fwb.12388.

Jin, S., L. Yang, P. Danielson, C. Homer, J. Fry, and G. Xian (2013), A comprehensive change detection method for updating the National Land Cover Database to circa 2011, *Remote Sens. Environ.*, *132*, 159–175, doi:10.1016/j.rse.2013.01.012.
Kelley, D. W., and E. A. Nater (2000), Historical sediment flux from three watersheds into Lake Pepin, Minnesota, USA, *J. Environ. Qual.*, *29*, 561–568, doi:10.2134/jeq2000.00472425002900020025x.
Kirkby, M. J. (1976), Tests of the random network model and its application to basin hydrology, *Earth Surf. Processes*, *1*, 197–212, doi:10.1002/esp.3290010302.
Lagasse, P. F., W. J. Spitz, L. W. Zevenbergen, and D. W. Zachmann (2004), Handbook for predicting stream meander migration, *Natl. Coop. Highway Res. Program Rep. 533*, 105 p., Transp. Res. Board of the Natl. Acad., Washington, D. C. [Available at http://onlinepubs.trb.org/onlinepubs/nchrp/nchrp_rpt_533.pdf, last accessed 24 May 2014.]
Lee, K. T., and C.-C. Yang (2010), Estimation of sediment yield during storms based on soil and watershed geomorphology characteristics, *J. Hydrol.*, *382*, 145–153, doi:10.1016/j.jhydrol.2009.12.025.
Leopold, L. B., M. G. Wolman, and J. P. Miller (1964), *Fluvial Processes in Geomorphology*, 544 pp., W. H. Freeman, San Francisco, Calif.
Marani, A., R. Rigon, and A. Rinaldo (1991), A note on fractal channel networks, *Water Resour. Res.*, *27*(12), 3041–3049, doi:10.1029/91WR02077.
Mantilla, R., V. K. Gupta, O. J. Mesa (2006), Role of coupled flow dynamics and real network structures on Hortonian scaling of peak flows, *J. Hydrol.*, *322*, 155–167, doi:10.1016/j.jhydrol.2005.03.022.
Mari, L., E. Bertuzzo, R. Casagrandi, M. Gatto, S. A. Levin, I. Rodriguez-Iturbe, and A. Rinaldo (2011), Hydrologic controls and anthropogenic drivers of the zebra mussel invasion of the Mississippi-Missouri river system, *Water Resour. Res.*, *47*, W03523, doi:10.1029/2010WR009920.
Marschner, F. J. (1974), *The Original Vegetation of Minnesota, a Map Compiled in 1930 by F.J. Marschner Under the Direction of M.L. Heinselman of the United States Forest Service*, map 1:500,000, Cartogr. Lab. of the Dep. of Geogr., Univ. of Minn., St. Paul.
McCluney, K. E., N. L. Poff, M. A. Palmer, J. H. Thorp, G. C. Poole, B. S. Williams, M. R. Williams, and J. S. Baron (2014), Riverine macrosystems ecology: sensitivity, resistance, and resilience of whole river basins with human alterations, *Front. Ecol. Environ.*, *12*(1), 48–58, doi:10.1890/120367.
McKay, L., et al. (2012), *NHDPlus Version 2: User Guide*, 181 pp., U.S. Environ. Prot. Agency, Washington, D. C. [Available at ftp://ftp.horizon-systems.com/nhdplus/nhdplusv21/documentation/nhdplusv2_user_guide.pdf, and last accessed 4 February 2015].
Mesa, O. J., and E. R. Mifflin (1986), On the relative role of hillslope and network geometry in hydrologic response, in *Scale Problems in Hydrology*, edited by V. K. Gupta, I. Rodriguez-Iturbe, and E. F. Wood, pp. 1–17, D. Reidel, Dordrecht, Holland.
Motta, D., J. D. Abad, E. J. Langendoen, and M. H. Garcia (2012), A simplified 2D model for meander migration with physically-based bank evolution, *Geomorphology*, *163–164*, 10–25, doi:10.1016/j.geomorph.2011.06.036.
Muneepeerakul, R., E. Bertuzzo, H. J. Lynch, W. F. Fagan, A. Rinaldo, and I. Rodriguez-Iturbe (2008), Neutral metacommunity models predict fish diversity patterns in Mississippi-Missouri basin, *Nature*, *453*, 220–222, doi:10.1038/nature06813.
Ojakangas, R. W., and C. L. Matsch (1982), *Minnesota's Geology*, 255 p., Univ. of Minn. Press, Minneapolis.
Paola, C., P. L. Hellert, and C. L. Angevine (1992), The large-scale dynamics of grain-size variation in alluvial basins, 1: Theory, *Basin Res.*, *4*(2), 73–90, doi:10.1111/j.1365–2117.1992.tb00145.x.
Parker, G. (2004), 1D aggradation and degradation of rivers: Normal flow assumption, chap. 14, in *1D Sediment Transport Morphodynamics With Applications to Rivers and Turbidity Currents*, 38 pp., Urbana, Ill. [Available at http://hydrolab.illinois.edu/people/parkerg//morphodynamics_e-book.htm, last accessed 20 May 2014.]
Parker, G., Y. Shimizu, G. V. Wilkerson, E. C. Eke, J. D. Abad, J. W. Lauer, C. Paola, W. E. Dietrich, and V. R. Voller (2011), A new framework for modeling the migration of meandering rivers, *Earth Surf. Processes Landforms*, *36*(1), 70–86, doi:10.1002/esp.2113.
Rinaldo, A., and I. Rodriguez-Iturbe (1996), Geomorphological theory of the hydrological response, *Hydrol. Processes*, *10*(6), 803–829, doi:10.1002/(SICI)1099-1085(199606)10:6<803::AID-HYP373>3.0.CO;2-N.
Rinaldo, A., A. Marani, and R. Rigon (1991), Geomorphological dispersion, *Water Resour. Res.*, *27*(4), 513–525, doi:10.1029/90WR02501.
Rinaldo, A., G. Botter, E. Bertuzzo, A. Uccelli, T. Settin, and M. Marani (2006), Transport at basin scales: 2. Applications, *Hydrol. Earth Syst. Sci.*, *10*, 31–48, doi:10.5194/hess-10–31-2006.
Rodriguez-Iturbe, I., and J. B. Valdes (1979), The geomorphologic structure of hydrologic response, *Water Resour. Res.*, *15*(6), 1409–1420, doi:10.1029/WR015i006p01409.
Schottler, S. P., J. Ulrich, P. Belmont, R. Moore, J. W. Lauer, D. R. Engstrom, and J. E. Almendinger (2014), Twentieth century agricultural drainage creates more erosive rivers, *Hydrol. Processes*, *28*(4), 1951–1961, doi:10.1002/hyp.9738.
Troutman, B. M., and M. R. Karlinger (1985), Unit hydrograph approximations assuming linear flow through topologically random channel networks, *Water Resour. Res.*, *21*(5), 743–754, doi:10.1029/WR021i005p00743.
U.S. Geological Survey (2014), *USGS Water Data for Minnesota*, U.S. Geol. Surv., Reston, Va. [Available at http://waterdata.usgs.gov/mn/nwis?, last accessed 20 May 2014.]
van de Lageweg, W. I., W. M. van Dijk, A. W. Baar, J. Rutten, and M. G. Kleinhans (2014), Bank pull or bar push: What drives scroll-bar formation in meandering rivers?, *Geology*, *42*(4), 319–322, doi:10.1130/G35192.1.
Wainwright, J. (2006), Degrees of separation: Hillslope-channel coupling and the limits of palaeohydrological reconstruction, *Catena*, *66*(1-2), 93–106, doi:10.1016/j.catena.2005.07.016.
Wilcock, P. (2009), Identifying sediment sources in the Minnesota River Basin, Rep. wq-b3–43, 16 p., Minn. Pollut. Control Agency, Mankato. [Available at http://www.pca.state.mn.us/index.php/view-document.html?gid=8099, last accessed 29 Apr 2014.]